A single-crystal copper (111) current collector for anode-free lithium batteries

Min-Ho Kim[1]†, Dong Yeon Kim[1]†, Yunqing Li[2,3], Jeongwoo Seo[1], Juyoung Kim[1], Myeong Seon Kim[1], Min Hyeok Kim[2,3], Taewon Kim[1], Ukhyun Jung[1], Sang-Wook Park[1], Rodney S. Ruoff[1,2,3,4]*, Dong-Hwa Seo[1,2]*, Sunghwan Jin[1]*, Hyun-Wook Lee[1]*

[1]School of Energy and Chemical Engineering, Ulsan National Institute of Science and Technology (UNIST), 50 UNIST-gil, Ulsan 44919, Republic of Korea

[2]Center for Multidimensional Carbon Materials (CMCM), Institute for Basic Science (IBS), Ulsan 44919, Republic of Korea

[3]School of Materials Science and Engineering, Ulsan National Institute of Science and Technology (UNIST), 50 UNIST-gil, Ulsan 44919, Republic of Korea

[4]Department of Chemistry, Ulsan National Institute of Science and Technology (UNIST), 50 UNIST-gil, Ulsan 44919, Republic of Korea

†These authors contributed equally

*Correspondence author. rsruoff@ibs.re.kr, dseo@unist.ac.kr, reachdream@unist.ac.kr, hyunwooklee@unist.ac.kr

Abstract

Anode-free lithium (Li) batteries that function via direct Li plating/stripping from cathodes have led to a surge of interest in metallic lithium as an ideal negative electrode. Despite its great promise, its practical use has been hampered by dendritic growth of Li metal, which results in low coulombic efficiencies and cell shorting. In addition, such dendritic growth of Li makes a larger unoccupied space in the battery, which causes dramatic reduction in volumetric energy density. We report that Li plating is a collective motion of Li adatoms influenced by the crystallographic orientation of the Cu substrate, and that Li adatoms can be redistributed by interacting with individual Cu grains via surface migration. By comparing centimeter-sized single-crystal Cu(111) and Cu(410) foils, we found that Cu(111) foil inhibits dendritic growth of metallic Li and that, per our modeling, this is likely due to the near-zero migration barrier of Li adatoms. We suggest that understanding, and 'controlling' the Li adatom surface migration 'behavior' opens a new avenue for achieving high-performance anode-free Li batteries.

Text

Ideally, *anode-free* lithium metal batteries (LMBs) should be at the forefront of high-energy density batteries through completely removing the metallic lithium (Li) anode in the initial states (*1*). In contrast to conventional battery systems, anode-free LMBs operate through direct Li plating/stripping on the Cu current collector without any other anode materials needed, such that the battery can, in principle, achieve the theoretical maximum energy density. Despite the excellent potential of LMBs as high-energy batteries, dendritic growth of metallic Li causes problems (*2*–*5*), such as low Coulombic efficiencies, rapid capacity fading, and internal short circuits, that have impeded their commercialization. Although the ideal configuration of anode-free LMBs has been discussed (*6*–*8*), the reported LMBs so far employed either a Li thin-film or a solid-state electrolyte, which are still in the early stages of development. One strategy includes designing compositions or additives in liquid electrolytes to inhibit the dendritic growth of Li. However, such modifications of liquid electrolytes can result in degradation of LMBs (*9*).

One approach to try to suppress the dendritic growth of Li in LMBs involves creating a homogeneous Li^+ flux condition throughout the metal current collector (*10*–*13*). During charging, since Li ions (Li^+) present in the liquid electrolyte are reduced to Li^0 and subsequently adsorbed on the substrate, achieving a uniform Li ion flux across the entire substrate is beneficial for the homogeneous and planar Li plating (*1*, *14*, *15*). In practice, however, it is reportedly almost impossible to achieve this condition due to diffusion-limited mass transport in the electrolyte (*16*). For example, when the formation of metallic Li is initiated by the charge transfer $Li^+ + e^- \rightarrow Li^0$ on the Cu current collector, the local distribution of Li ions within the liquid electrolyte deviates from its equilibrium, causing a concentration gradient of Li ions. As a result, heterogeneous Li^+ flux is accelerated by the local diffusion-limited reaction at the point where the concentration of

Li^+ goes to zero, resulting in a local steep concentration gradient of Li ions in the electrolyte. As a result, dendritic Li growth is triggered, which is commonly recognized in the Sand`s equation (*17*, *18*). Studies of attempts to relieve this local steep concentration gradient of Li ions in the electrolyte have included highly concentrated electrolytes (*19*, *20*), modified electrodes with lithiophilic property (*21*, *22*), and metallic alloying with heteroatoms (e.g., Si, Sn, Al, Mg, Ag, etc.) (*23–25*). These studies focused on Li adsorption but not on the surface migration of Li atoms that can take place after Li adsorption. A recent computational study suggested the possibility that the local electrodeposition of metals, described by the conventional Sand's equation, can be suppressed when the self-migration of metal atoms on anode surfaces is activated (*26*). However, this concept has not been proved experimentally and planar growth of Li remains challenging due to, especially, a lack of understanding of Li migration on typical Cu current collectors.

We studied and report here the adsorption and migration of Li during Li plating using centimeter-sized single crystal Cu foil as a current collector for anode-free batteries. We observed homogeneous & 2D growth of Li on single crystal Cu(111) foils with the complete absence of dendrites, but we found dendritic growth of Li on single crystal Cu(410) and polycrystalline Cu foils. We found through our theoretical modeling that the planar growth observed on Cu(111) foils is mainly due to a *near-zero migration barrier* for the migration of Li adatoms on the (111) surface. To the best of our knowledge, this is the first study that free surface migration of Li adatoms on single crystal substrate promotes lateral growth of Li. Given that the single crystal Cu(111) foils can be mass produced, our study suggests high-energy-density anode-free Li batteries are achievable could be commercialized reasonably soon.

Polycrystalline Cu foils, which have been widely used as metal current collectors for anode-free

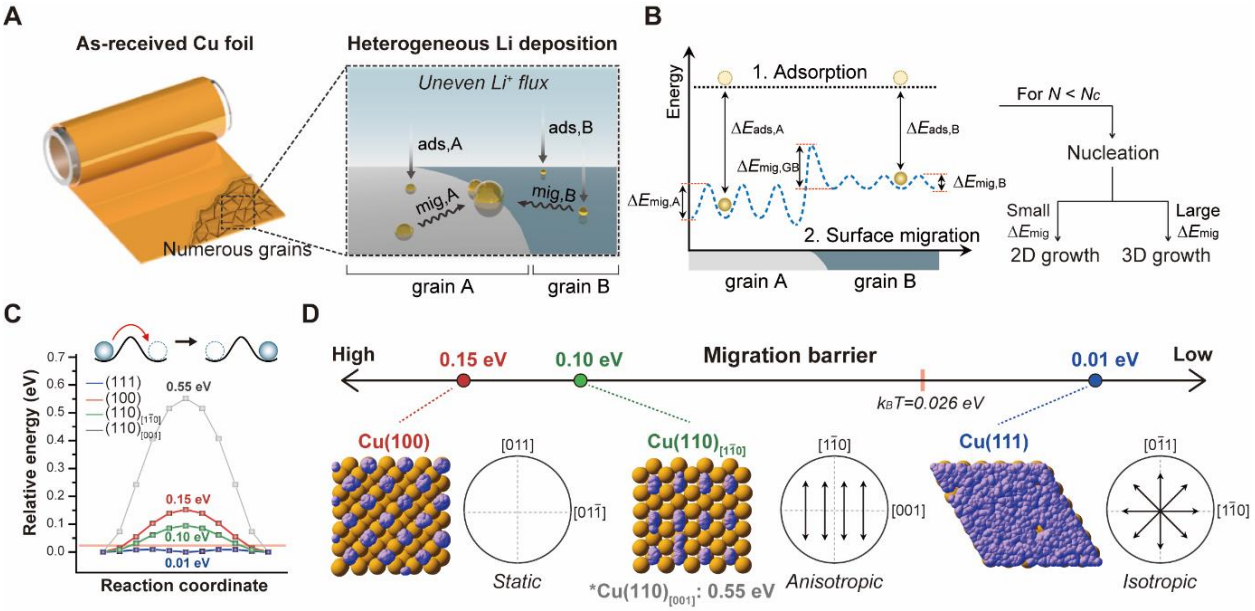

Fig. 1. Li plating phenomenon on a Cu substrate and computational modeling. (A) Schematics of Li plating behaviors on as-received Cu foil composed of numerous grains and grain boundaries (GBs)**,** and **(B)** the associated energy landscape. Nucleation of Li metal results from the adsorption and migration of Li atoms until the number of Li atoms on the surface, N, exceeds the critical value, N_c. After their adsorption, the surface migration of Li adatoms can significantly influence the growth mode (2D vs. 3D) of Li metal. Different interactions of Li atoms/adatoms for each grain result in heterogeneous Li plating behaviors. **(C)** Reaction energy profiles for the different Cu facets when the Li adatom diffuses to a neighboring site. **(D)** Different Cu plane orientations and the motion of Li adatoms depending on the Li migration barriers. On Cu(111) the Li migration barrier is less than the thermal energy at room temperature (k_BT = 0.026 eV), and the Li metal atoms migrate along the Cu surface rather than forming Li dendrites. All the trajectories of Li on each facet, computed by the *ab-initio* molecular dynamics (AIMD) simulation for 10 ps with a timestep of 2 fs at 500 K, are collected in single snapshots (Cu: light-brown and Li: purple).

batteries, consist of numerous grains with different crystallographic orientations (**Fig. 1A**). Since different grains and their boundaries have different energies depending on their atomic arrangements (*27*, *28*), we found different Li dynamics during the charging process. These Li dynamics including adsorption and surface migration, are determined by the interactions between Li atoms and individual grains (and their boundaries), as shown in their energy landscape (**Fig. 1B**). For example, suppose that grain A has significantly higher affinity for Li atoms/adatoms than grain B. Grain A strongly interacts with Li atoms such that Li atoms are adsorbed readily onto its surface (*29*). These adsorbed Li atoms diffuse on the surface of Cu foils and gather together to form Li clusters. As the size of the Li cluster exceeds the critical value, it eventually leads to nucleation of Li metal on the Cu foil (*30*). The nuclei on Grain A can grow in 3D since the Li

adatom surface migration (on the copper surface of grain A) is smaller. Grain B with lower Li affinity can induce planar Li plating on the Cu foil, by continuous redistribution of Li adatoms via active surface migration. Such grain-dependent Li dynamics is, we have found, the major reason why Li plating occurs heterogeneously on polycrystalline Cu foils.

Indeed, we thought that single crystal Cu(111) foil might possibly inhibit dendrite growth, and our initial experiments with anode-free cell configurations showed that lithium deposited and grew in a 2D manner on the Cu(111) foil, but dendrites grew (as also expected from a large body of literature on this topic) on polycrystalline Cu foils. This discovery motivated modeling of both the Li atom adsorption energy on different crystal facets of Cu as well as the barriers for surface migration on those facets. We discuss our modeling results next, and then return to a detailed discussion of experimental results.

To investigate how Li dynamics depends on the type of Cu facets, we selected three low-index Cu facets (Cu(100), Cu(110) and Cu(111)), and calculated their Li adsorption energies (E_{ads}) and migration activation energies (E_{mig}) through first-principles calculations. Please note that all calculations in this study were performed with no electrolyte present. As both the surface of Cu (and also Li atoms) cannot form chemical bonds with the electrolyte, we suggest that the electrolyte does not affect the results of our modeling. The calculated adsorption energies of Li atoms on Cu facets, which are examined through the Perdew-Burke-Ernzerhof (PBE) functional (*31*), are -2.23 eV for Cu(100), -2.36 eV for Cu(110), and -2.39 eV for Cu(111), that is, the Cu(111) facet has the lowest adsorption energy for Li atoms than other facets although its adsorption energy is close to that of the Cu(110) facet (**fig. S1**). On the other hand, the *surface migration* behaviors of Li adatoms on these facets, which were computed through the climbing image nudged elastic band (CI-NEB) calculation (*32*) and ab initio molecular dynamics (AIMD) simulation, show an entirely

different trend (**Fig. 1C and 1D and fig. S2**). Considering surface symmetry of each facet, the migration pathways for Cu(100) and Cu(111) are isotropic whereas that of Cu(110) is anisotropic toward [1-10] and [001] directions. NEB calculations of migration barriers of Li adatoms for each facet yield: 0.55 eV for Cu(110) to the [001] direction, 0.15 eV for Cu(100), 0.10 eV for Cu(110) to the [1-10] direction, and 0.01 eV for Cu(111); the migration barrier of Li adatoms diffusing on the Cu(111) facet is thus much lower than for other facets and even lower than the thermal vibration energy at room temperature (k_BT: 0.026 eV, where k_B is the Boltzmann's constant and T is the temperature). The Cu(111) facet has a negligible migration barrier for Li adatoms. AIMD simulation (**Fig. 1D)** shows that Li adatoms on Cu(111) move isotropically and their trajectories uniformly cover the surface of Cu(111), enabling planar Li growth. On the other hand, Li adatoms on the Cu(100) facet do not migrate and were found to be adsorbed and isolated onto equivalent sites nearby octahedral holes on its surface. When additional Li atoms are adsorbed onto Cu(100), we suggest these results show it likely to result in vertical growth rather than lateral growth of Li, because such Li atoms can be adsorbed onto the surface of pre-existing Li coated regions, without redistribution of Li adatoms on this facet's surface (*33*). We find that for the Cu(110) facet, Li adatoms move slowly toward the [1-10] direction due to its direction-dependent migration barrier. This anisotropic motion of Li adatoms should also yield, eventually, vertical growth. These calculations suggest that Li dynamics can be controlled if a 'single crystal substrate' with one crystallographic facet over the whole region is used, and that single crystal Cu(111) is particularly promising due to its near-zero migration barrier of Li adatoms. The migration barrier of Li into the bulk Cu is 0.68 eV (*34*), which is significantly higher than the migration barrier of Li at the surface. Considering that the probability of Li migration is inversely proportional to the exponent of the activation barrier of Li, Li plating behavior is mainly governed by the surface migration of Li, as

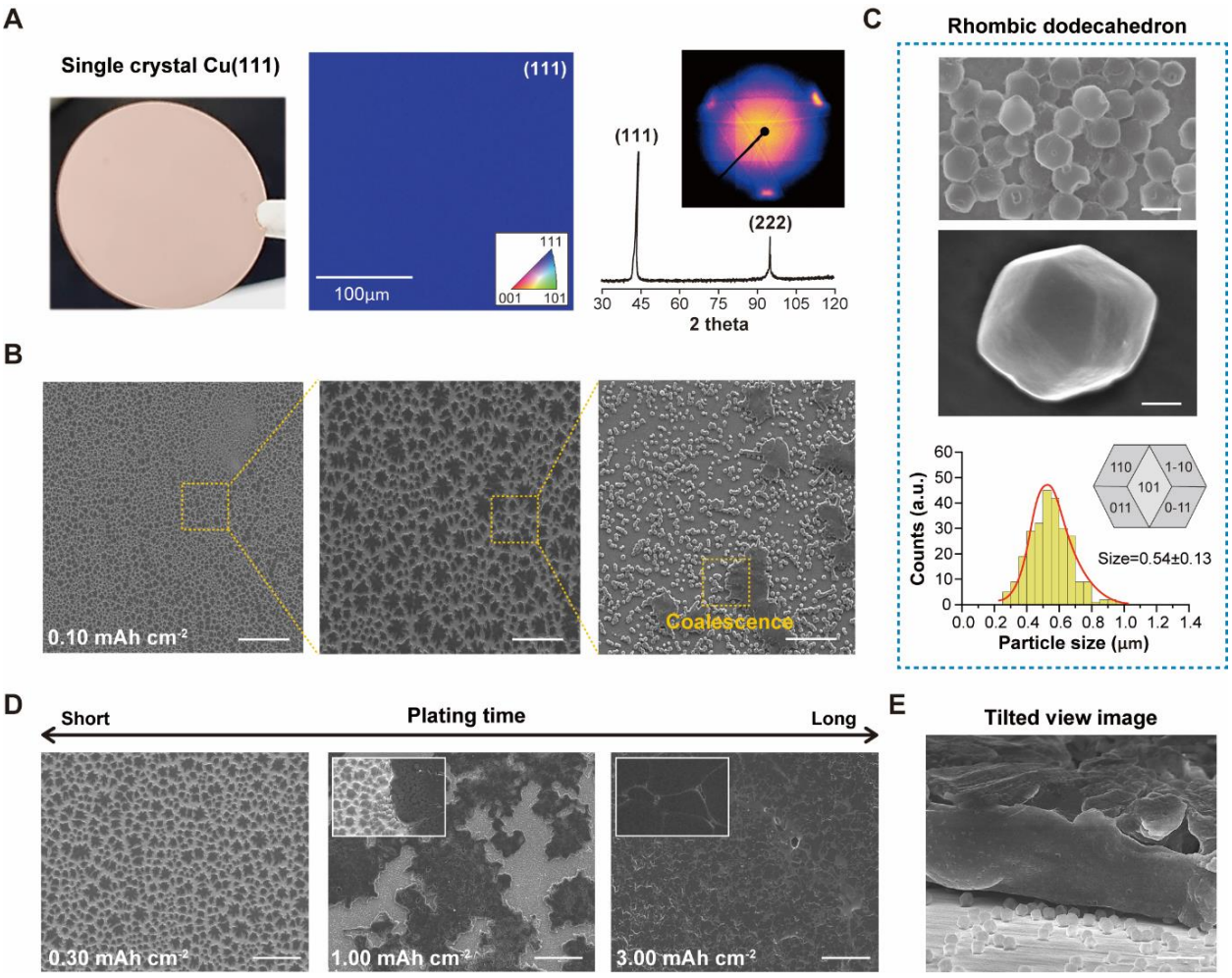

Fig. 2. Morphology of lithium deposited on single crystal Cu(111) foils. (A) Characterization of single crystal Cu(111) foils: digital photography of a 1.4 cm diameter foil (left), an EBSD inverse pole figure (IPF) map of the foil (middle), XRD 2θ scan and WAXS results (right). The single crystal foils have (111) surface orientation, as indicated by the uniform blue color in the IPF map, the {111} peaks in the XRD spectrum, and the triangle-shaped spots in WAXS. **(B)** SEM images of electrodeposited Li on a Cu(111) foil at an areal capacity of 0.10 mAh cm^{-2}. The scale bars are 200, 50, and 10 μm from left to right, respectively. (**C**) SEM images of rhombic dodecahedral Li particles (scale bars are 1 μm and 300 nm for top and bottom images, respectively) on Cu(111) foils along with their size distributions (mean = 54 ± 13 nm). **(D)** Top-view SEM images of electrodeposited Li on Cu(111) foils with capacities of 0.30, 1.00, and 3.00 mAh cm^{-2}. The scale bars are all 100 μm. **(E)** 70° tilted view SEM image of electrodeposited Li on Cu(111) foil at an areal capacity of 3.00 mAh cm^{-2}. The scale bar is 5 μm. All Li deposition experiments on Cu foils were conducted at a current density of 0.10 mA cm^{-2} in an electrolyte containing 1.3 M $LiPF_6$ in EC/DEC + 10% FEC.

we describe here.

To experimentally test Li dynamics on single crystal Cu(111) substate, we prepared large-area single crystal Cu(111) foils by the contact-free annealing (CFA) process, from commercially available polycrystalline Cu foils (*35*). Electron backscatter diffraction (EBSD), X-ray diffraction

(XRD) and wide-angle X-ray scattering (WAXS) results show our single crystal foils have (111) surface orientation over a large area (**Fig. 2A**). Using these Cu(111) foils, we assembled coin cells with Li metal and commercially available liquid electrolytes (1.3M $LiPF_6$ in ethylene carbonate (EC)/diethylene carbonate (DEC) 3:7+ 10% fluoroethylene carbonate (FEC)) and investigated Li plating behaviors on the surfaces of these foils. After Li plating with a capacity density of 0.10 mAh cm^{-2}, numerous 2D Li islands were observed on Cu(111) foils (**Fig. 2B)**. We found that these 2D islands were formed through coalescence of Li particles with an average size of 54 ± 13 nm, and most of these Li particles have a rhombic dodecahedron shape (**Fig. 2C and fig. S3**). It is commonly known that rhombic dodecahedral particles with Body-Centered Cubic (BCC) structure are formed by the surface energy minimization of the particles because all facets of the particle have only {110} planes with the lowest surface energy (*36–39*). Unlike free particles, the equilibrium shape of the particles on the substrate is influenced by the substrate (*40*). However, as shown in our simulation results, since the migration barrier of Li adatoms on Cu(111) surface is almost zero, Li adatoms should behave like free-particles on the Cu(111) surface. From this point of view, it seems that such rhombic dodecahedral particles on Cu(111) foils were formed by the surface energy of the particles as the main driving force. Upon further Li plating, Li islands consisting of rhombic dodecahedral particles continue to grow laterally and merge with each other to form larger Li islands (**Fig. 2D** and **fig. S4**). Both small rhombic dodecahedral Li particles and large Li islands seem to be only *partially* bound to the Cu(111) surface (**Fig. 2E)**, suggesting the adhesion between Li deposits and Cu(111) foils is not strong. Under standard coin cell operation, 2D planar growth of Li on the surface of Cu(111) foil was found to always occur, and 3D vertical growth was thus not observed.

To systematically evaluate Li plating behaviors depending on crystallographic planes of Cu, we

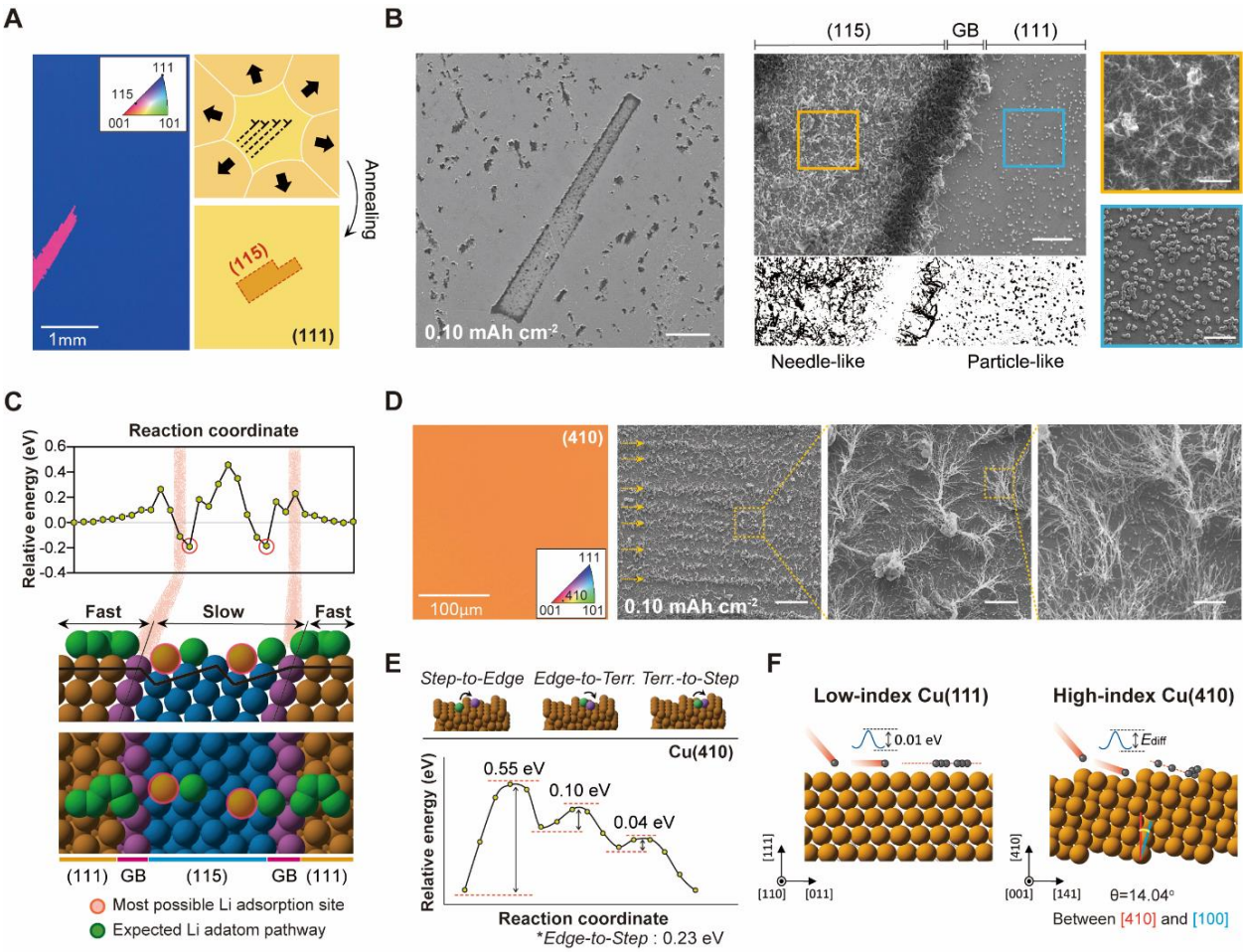

Fig. 3. Facet-dependent Li deposition. (A) Cu(111) foil embedded with (115) twin grains: EBSD IPF map (left) and schematic illustrating the formation of annealing twins (right). The twin grain has (115) surface orientation. Because the boundaries between (111) and (115) grains are particularly stable, (115) grains remain even after (111) grains consume surrounding grains and grow in size. **(B)** SEM images of Li electrodeposited on Cu(111) foils having (115) grains. With the aid of image-processing software (ImageJ), two distinct morphologies of Li deposits (indicated by the color black) can be distinguished: particle-like Li on (111) grains and needle-like Li on (115) grains. The scale bars are 500 μm (left), 20 μm (middle), and 5 μm (right, for both yellow and blue boxes), respectively. **(C)** Computational model of Cu surface composed of (111) and (115) grains, and their boundaries; relative energies of Li adatoms (top) and stable Li adsorption sites on this model surface (bottom). Li adatoms move faster on the (111) surface than on the (115) surface (Cu: brown, Li adatom: green, and Cu in GB: purple) **(D)** EBSD IPF map of single crystal Cu(410) foils (left) and top-view SEM images of Li electrodeposited on Cu(410) foils (right). The scale bars for SEM images are 100, 20, and 5 μm from left to right, respectively. **(E)** Calculated reaction energy profiles for migrationof Li adatoms on Cu(410) surface. *Step-to-Edge* is Li migration'from step to terrace edge', *Edge-to-Terr.* is Li migration 'within the terrace' and both *Terr.-to-step* and *Edge-to-Step* correspond to Li migration 'from terrace to step'. **(F)** Schematics of Li deposition behaviors on Cu(111) and Cu(410) surfaces; Li adatoms are expected to be uniformly distributed on the low-index surface, while they are confined to step sites on the high-index surface. All Li deposition experiments on Cu foils were conducted at a current density of 0.1 mA cm^{-2} in an electrolyte containing 1.3M $LiPF_6$ in EC/DEC = 3:7 + 10% FEC.

used 'special' Cu(111) foil that contains some grains with a (115) surface orientation ((115) grains). During contact free annealing, (115) grains (having a Σ3 twin relationship with respect

to the (111) plane) are sometimes present in Cu(111) foils by the formation of annealing twins (**Fig. 3A and fig. S5**) (*41*). These (115) grains are easily distinguished by scanning electron microscopy (SEM) and optical microscopy (OM), because they have a rectangular shape, length of several mm, and are well aligned with each other along the 3-fold symmetry of the parent (111) plane. The presence of such (115) grains allowed us to Li plating behaviors on them as well as on the (111) regions. After deposition of a small quantity of Li (0.1 mAh cm^{-2}) on this Cu(111) foil, Li was found to be primarily deposited at the boundary between the (115) and (111) grains (**Fig. 3B**). The amount of Li deposited at this grain boundary was much higher than inside grains, and the (115) grains had more deposited Li (per area) than the (111) grain. We found different morphologies of the Li deposited (plated) on each grain: particle-like Li (rhombic dodecahedrons as described above) deposits on the (111) grain but needle-like Li deposits on the (115) grain. This was true for another commonly used electrolyte (the electrolyte of 2M lithium bis(fluorosulfonyl)imide (LiFSI) in dimethyl ether (DME) + 2% $LiNO_3$, see **fig. S7**).

We performed density functional theory (DFT) calculation for Li migration on a modeled Cu substrate composed of (111) and (115) surfaces, and their boundary (**Fig. 3C and Supplementary movie S1**). We calculated the relative energies of Li adatoms at various positions on the substrate with reference to the Li adatom on the (111) surface far away from the boundary. On the (111) surface, the relative energies of Li adatoms according to their positions remain almost constant, indicating that Li adatoms can move freely on the (111) surface, due to the near-zero migration barrier for Li adatoms on the (111) surface, as shown in **Fig. 1C**. However, the relative energy of Li adatoms on the (111) surface begins to change as it approaches grain boundaries (GBs) and drops significantly when the Li adatom is located on the boundary. This implies that Li adatoms move freely on the (111) surface but eventually become stuck on the boundary (marked red circles

in **Fig. 3C**). These simulation results well correlate with the experimental observation that the Li deposits are concentrated at the GBs rather than inside the grains. In addition, the (115) surface exhibits a large variation of relative energy depending on the binding sites. Unlike the low index (111) surface, composed of a single large terrace, the (115) surface consists of multiple terraces and steps; the migration of Li adatoms is limited within the step sites since Li atoms/adatoms are preferentially adsorbed to the 'step' sites, and their migration out of the 'step' is restricted (**fig. S8**). This might be the main reason for the observed 3D growth on the (115) grain (**Fig. 3B**).

Single crystal Cu(410) foils were prepared from polycrystalline foils with the initial (100) texture by using the CFA process (*35*). We plated Li on these Cu(410) foils under the same conditions as for Cu(111) foils. Cu(410) foil shows needle-type growth consisting of numerous Li 'whiskers' that are connected by Li 'chunks' (**Fig. 3D** and **fig. S9A**); these Li deposits were mainly distributed in lines that are parallel to each other (marked by yellow arrows). Our EBSD results show that the crystallographic direction of these lines is [100] (**fig. S9B**). The observed Li deposits can be ascribed to the atomic structure of the (410) surface. The Cu(410) surface has stepped surface structure with (100) terraces and the crystallographic direction of these steps is [001]; the adsorption energy of Li atoms at the 'step' site is the larger than other possible adsorption sites on the terraces (**fig. S10**). Li atoms are likely to preferentially adsorb onto step sites in Cu(410) surfaces (this preferential adsorption of Li atoms onto step sites also occurs on the Cu(115) surface, see **fig. S8**). As shown in **Fig. 3E** the activation barrier for Li migration on the Cu(410) surface is significantly lower for the migration toward the steps than out of the steps, thus Li adatoms can be trapped mainly along the steps. This might be the reason why 3D Li was mainly deposited in rows along the [001] direction in our experiments. The Cu(410) foil contains some (223) grains that have a similar shape and size to the (115) grains in the Cu(111) foil (because they are also annealing

twins formed from the parent (410) grain). We found that the Li plating on the Cu(410) foil with (223) grains has plated Li 'crowded' on the (410) region but 'avoiding' the (223) grains (**fig. S11**). Since the (223) surface is close to the (111) surface, 3D plating of Li happen preferentially on (410) surface when we used Cu(410) foils with (223) grains.

From our observations and modeling, the crystallographic orientation of substrates is found to be a critical parameter influencing Li plating behavior in terms of amount of Li deposited and morphology (2D vs 3D) of the Li deposits. For example, Li adatoms on Cu(410) surfaces are non-uniformly adsorbed and their migration is limited (to mainly within the step regions), eventually leading to substantial vertical growth of Li deposits. Li adatoms on the Cu(111) surface are uniformly adsorbed and diffuse freely, allowing them to form 2D Li deposits uniformly distributed over the entire surface (**Fig. 3F**).

From our results and analysis, polycrystalline Cu foils having many different grains with various surface orientations inevitably induce severe dendritic Li growth along with non-homogenous Li plating, as has been reported about Li plating on polycrystalline Cu substrates (*42*, *43*). In general, as-received Cu foils have μm-scale surface roughness owing to rolling marks which are formed during their production. Such high roughness results in 3D agglomerates of Li aligned along the rolling marks (**fig. S12**). When rolling marks are removed through annealing or electropolishing, 3D agglomerates of Li were still observed on polycrystalline foils (**fig. S13 and S14**). These 3D Li deposits, significantly different from the 2D Li deposits on Cu(111) foils, were *always* observed on polycrystalline Cu foils, regardless of Li plating conditions (**fig. S15 to S18**). The presence of grains with high-index planes and GBs in polycrystalline foils, from our work here, seems to play a central role in such dendritic Li growth.

We assembled Cu|Li cells using ether-based, and carbonate-based, electrolytes and measured

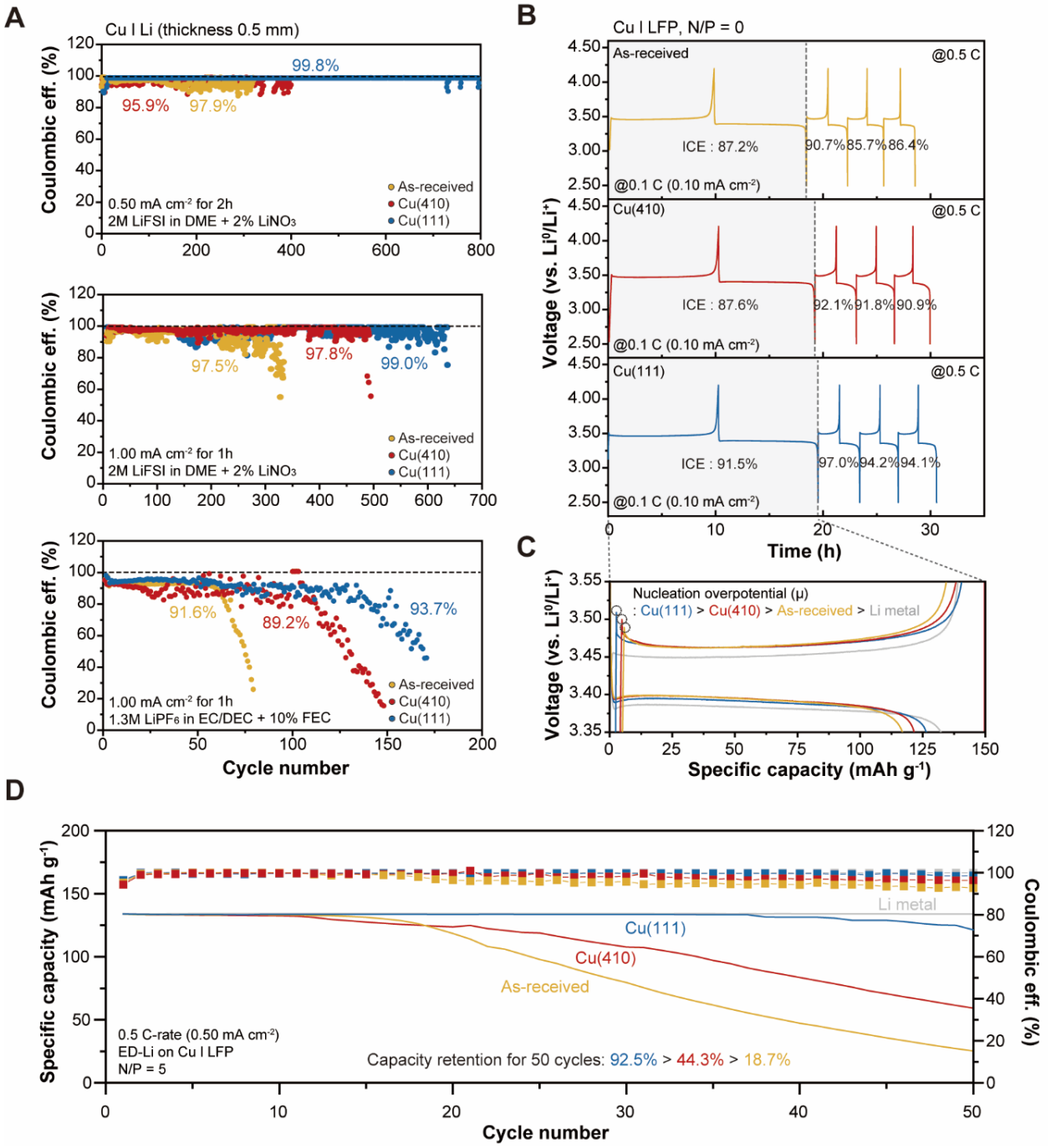

Fig. 4. Electrochemical performances of anodeless cells fabricated with as-received Cu, Cu(111), and Cu(410) foils. (A) CEs of Cu|Li cells: cycled at 0.50 mA cm^{-2} for 2h (top) and 1.00 mA cm^{-2} for 1h (middle) in ether-based electrolyte, and cycled at 1.00 mA cm^{-2} for 1h in carbonate-based electrolyte (bottom). $CE_{avg.}$ were calculated for the initial 50 cycles. **(B)** Voltage profiles during cycles for Cu|LFP cells. The initial cycle was operated at C/10-rate (0.10 mA cm^{-2}) and subsequent cycles were operated at C/2-rate (0.50 mA cm^{-2}). **(C)** Voltage hysteresis for Cu|LFP cells. The nucleation overpotentials (μ) for the Li plating is represented as black circles. **(D)** Cycle performances of ED-Li on Cu|LFP cells at the C/2-rate. In **(C)** and **(D)**, the gray lines (labeled as Li metal) correspond to Li|LFP cells fabricated by a thick Li metal foil as a counter electrode. All full-cell tests were conducted within the voltage range of 4.25–2.50 V in an electrolyte containing 1.3M $LiPF_6$ in EC/DEC + 10% FEC.

231 their electrochemical performances (**Fig. 4A and fig. S19 to S22**). In the ether-based electrolyte,

the cells using Cu(111) foils as substrates showed almost constant coulombic efficiencies (CE), which is defined as the ratio of discharge capacity to charge capacity. They showed $CE_{avg.}$ of 99.8 % (up to 800 cycles) and 99.0 % (up to 500 cycles) when each cycle was operated at a current density of 0.50 mA cm^{-2} for 2 h and 1.00 mA cm^{-2} for 1 h, respectively. The cells with as-received Cu and Cu(410) foils showed much lower CE with large fluctuation. For the first 50 cycles, the cell with as-received Cu foil showed CE of 97.9 % when each cycle was operated at 0.50 mA cm^{-2} for 2 h and 97.5 % when each cycle was operated at 1.00 mA cm^{-2} for 1 h, and the cell with Cu(410) foil showed CE of 95.9 % and 97.8%, respectively, at these same operating conditions. After 50 cycles, the cells with as-received Cu and Cu(410) foils showed rapid CE decay. Such lower CE and sudden decay of CE might be mainly attributed to dendritic growth of Li occurring on both as-received Cu and Cu(410) foils. Since the dendritic Li on as-received Cu and Cu(410) foils has a much larger surface area than the planar Li on the Cu(111) foil, side-reactions with electrolyte are aggravated, resulting in the poor CE and cyclability (*3*, *44*). Likewise, the cells with carbonate-based electrolytes, which generally have lower CE than the ether-based electrolyte systems due to their higher reactivity to Li (*15*), showed similar results for CE: the cells with Cu(111) foils have superior performances than those with as-received Cu and Cu(410) foils.

To further test the feasibility of our single crystal foils for anode-free systems, we assembled Cu|$LiFePO_4$ (LFP) cells using carbonate-based electrolyte and measured their electrochemical performances (**Fig. 4B and C**). Different from 'nearly infinite' Li supply from a Li metal counter electrode (0.5 mm) in Li|LFP cells, the Li supplied in Cu|LFP cells is from the LFP cathode. The cyclic performances of Cu|LFP cells are *entirely* determined by electrochemical reversibility of Li deposited on the Cu substrate (*44*, *45*), revealing the effect of Cu substrate more clearly. The initial CEs (ICEs; CE during 1^{st} cycle) of the cell with Cu(111) foil was 91.5 % compared to cells with

as-received Cu (87.2 %) and Cu(410) (87.6 %) foils. Such trend in which the cell using Cu(111) foil exhibited highest CE, was also observed in subsequent cycles. **Figure 4C and fig. S23A** show enlarged voltage-capacity profiles of each cell at the 1st cycle that more clearly show the voltage corresponding to the highest peak value at the beginning of the charging. These voltages are known as *relative nucleation overpotentials*, which represent whether Li can be easily plated at the initial stage (*42*). The overpotentials of the full-cells decreased as Cu(111) > Cu(410) > as-received Cu foils. The highest overpotential appearing in the cell with Cu(111) foil suggests that nucleation of Li plating on the Cu(111) surface is more difficult than other surfaces. This can be understood based on adsorption/migration behaviors of Li atoms on low-index versus high-index Cu surfaces. High-index surfaces have *terraces with low-index surfaces* and *steps*. As shown in our simulation results for high-index surfaces (for example, Cu(115) and Cu(410) surfaces), the adsorption energy at step regions is much lower than the terrace regions, therefore, the adsorption of Li atoms mainly occurs at the steps in the high index-facets; and the surface migration of these adsorbed adatoms is limited within the steps. Considering that nucleation occurs when atoms adsorbed to the surface bond or bind to each other to generate a cluster of n atoms with n above a critical value, the limited Li adsorption/migration at step regions in high-index facets favors nuclei forming. Similarly, the adsorption/migration of Li atoms in as-received Cu foils occurs first at GBs and step regions of grains with high-index surfaces. On Cu(111) surfaces Li adatoms are adsorbed uniformly and readily diffuse on this surface and nucleation is less likely. The near-zero migration barrier for surface migration of Li atoms on Cu(111) might also favor Li-Cu adhesion over Li-Li cohesion in the initial nucleation stage. For these reasons the Cu(111) foils has the highest nucleation overpotential compared to the other Cu foils. Our observation of full coverage of Li on the Cu(111) foils but not on the as-received and Cu(410) foils is further evidence of such substrate-dependent

nucleation behaviors.

How flat and smooth are our Cu(111) foils? We have found by AFM that they have remarkably large terrace regions and that the steps are typically single-atom steps(*35*, *46*). We suggest there are possibilities for lowering the relative nucleation overpotential of our Cu(111) foils, such as: (*i*) altering the step density, (*ii*) 'decorating' the steps and/or terraces with heteroatoms (adsorbed and/or substitutional in the surface); that favor nucleating Li clusters.

We compared cycling performance of Cu|LFP cells with N/P ratio of 0 (**fig. S23B and C**), which is close to the ideal condition for anode-free systems (here, N/P ratio indicates the ratio of the capacity of the negative electrode to that of the positive electrode; that is, N/P=0 indicates that the battery operates with only Li source in positive electrode). The cells with Cu(111) foils show better CE and cyclability over the cells with as-received and Cu(410) foils. However, all these cells are degraded significantly after some number of cycles and this could be due to severe side reactions of Li with carbonate-based electrolytes (*15*). We pre-electrodeposited Li ((ED-Li) on Cu foils and assembled ED-Li on Cu|LFP cells with N/P ratio of 5 (**Fig. 4D**); here, even if side reactions between Li and electrolytes occurs, the cell lifetimes can be extended until the available ED-Lis on the Cu substrates are entirely consumed, unless cell shorting due to dendritic growth of Li happens (*47*). The cell with Cu(111) foil showed capacity retention of 92.45 % at 50 cycles, but the cells with as-received Cu and Cu(410) foils show poor cycling with capacity retention of 44.28 % and 18.67 %, respectively, for 50 cycles. These results show that the dissipation of ED-Li on Cu(111) foils is much slower than on as-received Cu and Cu(410) foils. Such differences can be attributed to the different Li morphologies of Li plated on these Cu foils during cycles. Compared to 3D Li grown on as-received Cu foils and on Cu(410) foils, 2D Li with a smaller surface area on Cu(111) foils minimizes the formation of 'dead' Li (that is, electrically inactive Li) and side

reaction with electrolytes, yielding much better cell cyclability. (We suggest that 'conventional wisdom' in the battery community that large nucleation overpotentials result in poor cell cyclability (*48–50*) be revisited, based on our report here.)

In conclusion, we discovered uniform 2D plating and the complete absence of dendritic growth on Cu(111) foils in anode-free Li battery cells, and our concurrent studies of as-received polycrystalline Cu foils (with, and without, rolling marks) and Cu(410) foils, show that Li deposits preferentially at grain boundaries and steps (and generally, on high index facets vs low index facets).Our modeling shows that surface migration on Cu(111) occurs almost barrier free, and this induces lateral growth of Li, instead of vertical dendritic growth. We suggest that our work described here provides a new opportunity(ies) for both high-energy lithium batteries including anode-free, and solid-state batteries.

References

1. J. Zhang, W. Xu, J. Xiao, X. Cao, J. Liu, Lithium Metal Anodes with Nonaqueous Electrolytes. *Chem. Rev.* **120**, 13312–13348 (2020).

2. Z. Zhang, Y. Li, R. Xu, W. Zhou, Y. Li, S. T. Oyakhire, Y. Wu, Capturing the swelling of solid-electrolyte interphase in lithium metal batteries. *Science (80-.).* **70**, 66–70 (2022).

3. X. He, D. Bresser, S. Passerini, F. Baakes, U. Krewer, J. Lopez, C. T. Mallia, Y. Shao-Horn, I. Cekic-Laskovic, S. Wiemers-Meyer, F. A. Soto, V. Ponce, J. M. Seminario, P. B. Balbuena, H. Jia, W. Xu, Y. Xu, C. Wang, B. Horstmann, R. Amine, C.-C. Su, J. Shi, K. Amine, M. Winter, A. Latz, R. Kostecki, The passivity of lithium electrodes in liquid electrolytes for secondary batteries. *Nat. Rev. Mater.* **6**, 1036–1052 (2021).

4. G. Zheng, S. W. Lee, Z. Liang, H.-W. W. Lee, K. Yan, H. Yao, H. Wang, W. Li, S. Chu, Y. Cui, Interconnected hollow carbon nanospheres for stable lithium metal anodes. *Nat. Nanotechnol.* **9**, 618–623 (2014).

5. Y. Jin, Z. Zheng, D. Wei, X. Jiang, H. Lu, L. Sun, F. Tao, D. Guo, Y. Liu, J. Gao, Y. Cui, Detection of Micro-Scale Li Dendrite via H2 Gas Capture for Early Safety Warning. *Joule*, 1–16 (2020).

6. J. Qian, B. D. Adams, J. Zheng, W. Xu, W. A. Henderson, J. Wang, M. E. Bowden, S. Xu, J. Hu, J. G. Zhang, Anode-Free Rechargeable Lithium Metal Batteries. *Adv. Funct. Mater.* **26**, 7094–7102 (2016).

7. W. Huang, C. Zhao, P. Wu, H. Yuan, W. Feng, Z. Liu, Y. Lu, S. Sun, Z. Fu, J. Hu, S. Yang, J. Huang, Q. Zhang, Anode-Free Solid-State Lithium Batteries: A Review. *Adv.*

Energy Mater. **12**, 2201044 (2022).

8. Y. G. Lee, S. Fujiki, C. Jung, N. Suzuki, N. Yashiro, R. Omoda, D. S. Ko, T. Shiratsuchi, T. Sugimoto, S. Ryu, J. H. Ku, T. Watanabe, Y. Park, Y. Aihara, D. Im, I. T. Han, High-energy long-cycling all-solid-state lithium metal batteries enabled by silver–carbon composite anodes. *Nat. Energy*. **5**, 299–308 (2020).

9. A. J. Louli, A. Eldesoky, R. Weber, M. Genovese, M. Coon, J. DeGooyer, Z. Deng, R. T. White, J. Lee, T. Rodgers, R. Petibon, S. Hy, S. J. H. Cheng, J. R. Dahn, Diagnosing and correcting anode-free cell failure via electrolyte and morphological analysis. *Nat. Energy*. **5**, 693–702 (2020).

10. Z. Liang, G. Zheng, C. Liu, N. Liu, W. Li, K. Yan, H. Yao, P.-C. Hsu, S. Chu, Y. Cui, Polymer Nanofiber-Guided Uniform Lithium Deposition for Battery Electrodes. *Nano Lett.* **15**, 2910–2916 (2015).

11. Y. Lu, M. Tikekar, R. Mohanty, K. Hendrickson, L. Ma, L. A. Archer, Stable cycling of lithium metal batteries using high transference number electrolytes. *Adv. Energy Mater.* **5**, 1–7 (2015).

12. W. Liu, D. Lin, A. Pei, Y. Cui, Stabilizing Lithium Metal Anodes by Uniform Li-Ion Flux Distribution in Nanochannel Confinement. *J. Am. Chem. Soc.* **138**, 15443–15450 (2016).

13. H. Chen, A. Pei, J. Wan, D. Lin, R. Vilá, H. Wang, D. Mackanic, H.-G. Steinrück, W. Huang, Y. Li, A. Yang, J. Xie, Y. Wu, H. Wang, Y. Cui, Tortuosity Effects in Lithium-Metal Host Anodes. *Joule*. **4**, 938–952 (2020).

14. X. B. Cheng, R. Zhang, C. Z. Zhao, Q. Zhang, Toward Safe Lithium Metal Anode in

Rechargeable Batteries: A Review. *Chem. Rev.* **117**, 10403–10473 (2017).

15. M. D. Tikekar, S. Choudhury, Z. Tu, L. A. Archer, Design principles for electrolytes and interfaces for stable lithium-metal batteries. *Nat. Energy*. **1**, 16114 (2016).

16. J. Xiao, How lithium dendrites form in liquid batteries. *Science (80-.).* **366**, 426–427 (2019).

17. C. Brissot, M. Rosso, J. N. Chazalviel, P. Baudry, S. Lascaud, In situ study of dendritic growth in lithium/PEO-salt/lithium cells. *Electrochim. Acta*. **43**, 1569–1574 (1998).

18. P. Bai, J. Li, F. R. Brushett, M. Z. Bazant, Transition of lithium growth mechanisms in liquid electrolytes. *Energy Environ. Sci.* **9**, 3221–3229 (2016).

19. J. Qian, W. A. Henderson, W. Xu, P. Bhattacharya, M. Engelhard, O. Borodin, J.-G. Zhang, High rate and stable cycling of lithium metal anode. *Nat. Commun.* **6**, 6362 (2015).

20. S. Chen, J. Zheng, D. Mei, K. S. Han, M. H. Engelhard, W. Zhao, W. Xu, J. Liu, J. Zhang, High-Voltage Lithium-Metal Batteries Enabled by Localized High-Concentration Electrolytes. *Adv. Mater.* **30**, 1706102 (2018).

21. D. Lin, Y. Liu, Z. Liang, H.-W. Lee, J. Sun, H. Wang, K. Yan, J. Xie, Y. Cui, Layered reduced graphene oxide with nanoscale interlayer gaps as a stable host for lithium metal anodes. *Nat. Nanotechnol.* **11**, 626–632 (2016).

22. W. Go, M. H. Kim, J. Park, C. H. Lim, S. H. Joo, Y. Kim, H. W. Lee, Nanocrevasse-Rich Carbon Fibers for Stable Lithium and Sodium Metal Anodes. *Nano Lett.* **19**, 1504–1511 (2019).

23. K. Yan, Z. Lu, H.-W. Lee, F. Xiong, P.-C. Hsu, Y. Li, J. Zhao, S. Chu, Y. Cui, Selective

deposition and stable encapsulation of lithium through heterogeneous seeded growth. *Nat. Energy*. **1**, 16010 (2016).

24. Z. Liang, D. Lin, J. Zhao, Z. Lu, Y. Liu, C. Liu, Y. Lu, H. Wang, K. Yan, X. Tao, Y. Cui, Composite lithium metal anode by melt infusion of lithium into a 3D conducting scaffold with lithiophilic coating. *Proc. Natl. Acad. Sci.* **113**, 2862–2867 (2016).

25. M. Wan, S. Kang, L. Wang, H. W. Lee, G. W. Zheng, Y. Cui, Y. Sun, Mechanical rolling formation of interpenetrated lithium metal/lithium tin alloy foil for ultrahigh-rate battery anode. *Nat. Commun.* **11**, 1–10 (2020).

26. F. Hao, A. Verma, P. P. Mukherjee, Electrodeposition stability of metal electrodes. *Energy Storage Mater.* **20**, 1–6 (2019).

27. L. Vitos, A. V. Ruban, H. L. Skriver, J. Kollár, The surface energy of metals. *Surf. Sci.* **411**, 186–202 (1998).

28. Y. N. Wen, J. M. Zhang, Surface energy calculation of the fcc metals by using the MAEAM. *Solid State Commun.* **144**, 163–167 (2007).

29. C. Xiao, B. A. Lu, P. Xue, N. Tian, Z. Y. Zhou, X. Lin, W. F. Lin, S. G. Sun, High-Index-Facet- and High-Surface-Energy Nanocrystals of Metals and Metal Oxides as Highly Efficient Catalysts. *Joule*. **4**, 2562–2598 (2020).

30. A. Pimpinelli, J. Villain, *Physics of Crystal Growth* (Cambridge University Press, 1998; https://www.cambridge.org/core/product/identifier/9780511622526/type/book).

31. J. P. Perdew, K. Burke, M. Ernzerhof, Generalized Gradient Approximation Made Simple. *Phys. Rev. Lett.* **77**, 3865–3868 (1996).

32. G. Henkelman, B. P. Uberuaga, H. Jónsson, Climbing image nudged elastic band method for finding saddle points and minimum energy paths. *J. Chem. Phys.* **113**, 9901–9904 (2000).

33. X. Gao, Y. N. Zhou, D. Han, J. Zhou, D. Zhou, W. Tang, J. B. Goodenough, Thermodynamic Understanding of Li-Dendrite Formation. *Joule*. **4**, 1864–1879 (2020).

34. R. Rupp, B. Caerts, A. Vantomme, J. Fransaer, A. Vlad, Lithium Diffusion in Copper. *J. Phys. Chem. Lett.* **10**, 5206–5210 (2019).

35. S. Jin, M. Huang, Y. Kwon, L. Zhang, B.-W. Li, S. Oh, J. Dong, D. Luo, M. Biswal, B. V. Cunning, P. V. Bakharev, I. Moon, W. J. Yoo, D. C. Camacho-Mojica, Y.-J. Kim, S. H. Lee, B. Wang, W. K. Seong, M. Saxena, F. Ding, H.-J. Shin, R. S. Ruoff, Colossal grain growth yields single-crystal metal foils by contact-free annealing. *Science (80-.).* **362**, 1021–1025 (2018).

36. X. Zhang, C. Dong, J. Zapien, S. Ismathullakhan, Z. Kang, J. Jie, X. Zhang, J. Chang, C.-S. Lee, S.-T. Lee, Polyhedral Organic Microcrystals: From Cubes to Rhombic Dodecahedra. *Angew. Chemie*. **121**, 9285–9287 (2009).

37. A. Hagopian, M.-L. Doublet, J.-S. Filhol, Thermodynamic origin of dendrite growth in metal anode batteries. *Energy Environ. Sci.* (2020), doi:10.1039/d0ee02665d.

38. Y. X. Chen, S. P. Chen, Z. Y. Zhou, N. Tian, Y. X. Jiang, S. G. Sun, Y. Ding, L. W. Zhong, Tuning the shape and catalytic activity of Fe nanocrystals from rhombic dodecahedra and tetragonal bipyramids to cubes by electrochemistry. *J. Am. Chem. Soc.* **131**, 10860–10862 (2009).

39. D. T. Boyle, Y. Li, A. Pei, R. A. Vilá, Z. Zhang, P. Sayavong, M. S. Kim, W. Huang, H. Wang, Y. Liu, R. Xu, R. Sinclair, J. Qin, Z. Bao, Y. Cui, Resolving Current-Dependent Regimes of Electroplating Mechanisms for Fast Charging Lithium Metal Anodes. *Nano Lett.* (2022), doi:10.1021/acs.nanolett.2c02792.

40. W. L. Winterbottom, Equilibrium shape of a small particle in contact with a foreign substrate. *Acta Metall.* **15**, 303–310 (1967).

41. N. Bozzolo, M. Bernacki, Viewpoint on the Formation and Evolution of Annealing Twins During Thermomechanical Processing of FCC Metals and Alloys. *Metall. Mater. Trans. A Phys. Metall. Mater. Sci.* **51**, 2665–2684 (2020).

42. A. Pei, G. Zheng, F. Shi, Y. Li, Y. Cui, Nanoscale Nucleation and Growth of Electrodeposited Lithium Metal. *Nano Lett.* **17**, 1132–1139 (2017).

43. P. Zou, Y. Wang, S.-W. Chiang, X. Wang, F. Kang, C. Yang, Directing lateral growth of lithium dendrites in micro-compartmented anode arrays for safe lithium metal batteries. *Nat. Commun.* **9**, 464 (2018).

44. D. T. Boyle, W. Huang, H. Wang, Y. Li, H. Chen, Z. Yu, W. Zhang, Z. Bao, Y. Cui, Corrosion of lithium metal anodes during calendar ageing and its microscopic origins. *Nat. Energy* (2021), doi:10.1038/s41560-021-00787-9.

45. C. Fang, J. Li, M. Zhang, Y. Zhang, F. Yang, J. Z. Lee, M.-H. Lee, J. Alvarado, M. A. Schroeder, Y. Yang, B. Lu, N. Williams, M. Ceja, L. Yang, M. Cai, J. Gu, K. Xu, X. Wang, Y. S. Meng, Quantifying inactive lithium in lithium metal batteries. *Nature*. **572**, 511–515 (2019).

46. D. Luo, X. Wang, B. Li, C. Zhu, M. Huang, L. Qiu, M. Wang, S. Jin, M. Kim, F. Ding, R. S. Ruoff, The Wet-Oxidation of a Cu(111) Foil Coated by Single Crystal Graphene. *Adv. Mater.* **33**, 2102697 (2021).

47. H. Wang, Y. Li, Y. Li, Y. Liu, D. Lin, C. Zhu, G. Chen, A. Yang, K. Yan, H. Chen, Y. Zhu, J. Li, J. Xie, J. Xu, Z. Zhang, R. Vilá, A. Pei, K. Wang, Y. Cui, Wrinkled Graphene Cages as Hosts for High-Capacity Li Metal Anodes Shown by Cryogenic Electron Microscopy. *Nano Lett.* **19**, 1326–1335 (2019).

48. R. Zhang, X. R. X. X.-R. Chen, X. R. X. X.-R. Chen, X. B. Cheng, X.-Q. Q. Zhang, C. Yan, Q. Zhang, Lithiophilic Sites in Doped Graphene Guide Uniform Lithium Nucleation for Dendrite-Free Lithium Metal Anodes. *Angew. Chemie Int. Ed.* **56**, 7764–7768 (2017).

49. Y. Gu, H. Y. Xu, X. G. Zhang, W. W. Wang, J. W. He, S. Tang, J. W. Yan, D. Y. Wu, M. Sen Zheng, Q. F. Dong, B. W. Mao, Lithiophilic Faceted Cu(100) Surfaces: High Utilization of Host Surface and Cavities for Lithium Metal Anodes. *Angew. Chemie - Int. Ed.* **58**, 3092–3096 (2019).

50. W. Ye, F. Pei, X. Lan, Y. Cheng, X. Fang, Q. Zhang, N. Zheng, D. L. Peng, M. S. Wang, Stable Nano-Encapsulation of Lithium Through Seed-Free Selective Deposition for High-Performance Li Battery Anodes. *Adv. Energy Mater.* **1902956**, 1–10 (2020).